

Fig. 2: Calibrated TCAD characteristics of the TT transistor against PDK data: (a)  $V_{DS} = 0.05V$  (b)  $V_{DS} = V_{DD}$ . For comparison the characteristics of the slow-slow (SS) and the fast-fast (FF) corner transistors obtained from the PDK are also plotted.  $T=300K$  (a.u. stands for arbitrary units).

the adjustments of the doping profiles and the transistor structure to match the electrostatic behavior of the TT transistors, which includes the threshold voltage ( $V_t$ ), the Subthreshold Slope (SS), the Drain Induced Barrier Lowering (DIBL) at different bias conditions and their dependence on the transistor dimensions. This is followed by carrier mobility calibration aiming to represent accurately the transistor performance at low and high drain biases. The mobility models (Philips unified mobility model [9], Lombardi model [10], and Hansch [11] model) are selected to represent as accurately as possible the temperature dependence. An example of such a TCAD simulated characteristics obtained for a TT  $n$ -channel transistor calibrated to TT transistor data from the PDK is illustrated in Fig. 2. For comparison, the characteristics of the slow-slow (SS) and the fast-fast (FF) transistors as obtained from the room temperature PDK are also plotted in the figure. For this particular demo, we have used 22nm FDSOI devices [12], but the methodology presented is generic and not dependent on a particular device architecture, technology node, or compact model.

### III. TT TRANSISTOR TCAD MODEL ADJUSTMENT

Next, we compare the room temperature characteristics of the TT transistor from TCAD (Fig. 2) and the corresponding measured data from a fabricated silicon wafer as illustrated in Fig. 3 (a). As expected, the measured transistor data is shifted with respect to the corresponding TT transistor. The TT transistor represents the average transistor characteristics across the wafer, across the lots and from lot to lot. The actual

transistor characteristics on each wafer are different from the average transistor characteristics due to uncontrollable variations in the fabrication conditions. The main process parameters that are causing the process variation are the dose and energy of different implantation steps, the gate oxide thickness, the annealing temperatures, and the transistor dimensions. Typically, up to 5%-10% variations in the above process parameters are expected during the fabrication process. The different technology parameters have different impact on threshold voltage, electrostatic integrity and drive current and should be carefully tested and combined to give the desirable shift in transistor behavior from the TT to the measured transistor. The result from the simulation of the process calibrated structure (in order to match the room temperature measurement) is illustrated in Fig. 3 (b). The new TCAD deck represents a Shifted TT (STT) transistor, which will be used at the next stage to perform calibration of the mobility, density gradient (for quantum correction), and other cryogenic specific models at cryogenic temperatures.

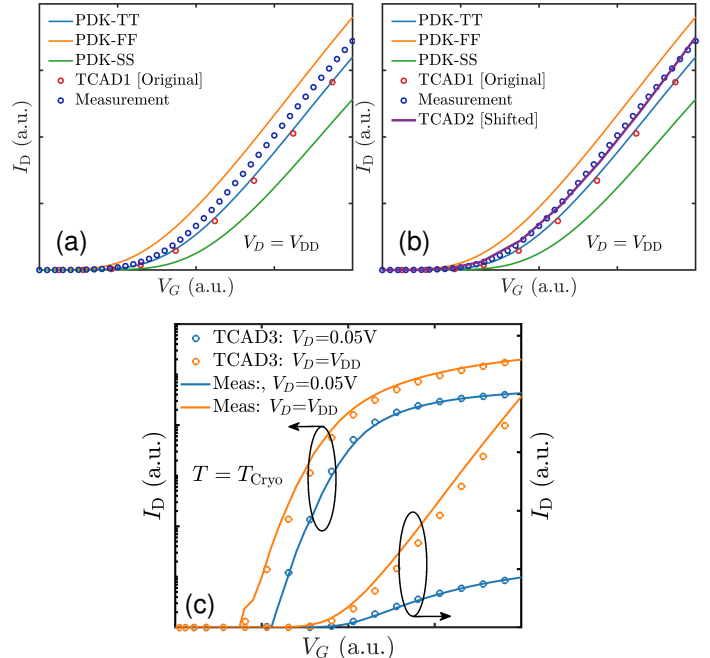


Fig. 3: (a) Comparison of  $I_{DS} - V_{GS}$  characteristics of the TT transistor in Fig. 2 and the corresponding measurement data at  $T=300K$ . (b) Comparison between the measurement data on a fabricated silicon wafer and the calibrated shifted TCAD model.  $T=300K$ . (c) Comparison between the measurement data and the calibrated shifted TCAD model both at cryogenic temperature ( $T_{Cryo}$ ) at low and high drain biases.

### IV. ADJUSTED TRANSISTOR AT CRYOGENIC TEMPERATURE

At this stage, the STT TCAD transistor simulations are calibrated to the cryogenic transistor measurements. The process includes two steps – electrostatic calibration and mobility calibration. The electrostatic calibration aims to reproduce  $V_t$ , SS, and DIBL of the STT at the cryogenic temperature ( $T_{Cryo}$ ). Considering the impact of the band tail states [13]

was critical for calibrating the subthreshold characteristics. The mobility calibration follows the calibration procedure at room temperature aiming to reproduce the current voltage characteristics above and below threshold. The results from the calibration of the STT transistor at  $T_{\text{Cryo}}$  are illustrated in Fig. 3 (c).

## V. TARGET DATA GENERATION AT CRYOGENIC TEMPERATURE AND MODEL EXTRACTION

After the calibration of the STT transistor, the TCAD structure of the ‘original’ TT transistor is used along with the calibrated band tail, incomplete ionization and mobility models at cryogenic temperature from the previous step to generate the target characteristics for the compact model [14] extraction of the TT transistor at cryogenic temperature. The model cards for the compact model are extracted to yield the cryogenic PDK using standard compact model extraction procedures. The generated target characteristics at cryogenic temperature and the extracted compact model (HSPICE [15] results) of the TT transistor are illustrated in Fig. 4.

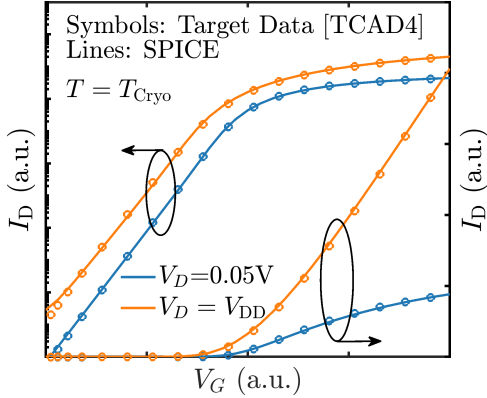


Fig. 4: Comparison between the target  $I_{\text{DS}} - V_{\text{GS}}$  data obtained from TCAD simulation of the original TT transistor at cryogenic temperature and the extracted compact model at low and high drain biases.

The same approach is applied to the FF and SS corners. We have also developed a Monte-Carlo (MC) approach to consider variability in the cryogenic PDK, which will be described in a future publication.

## VI. CONCLUSIONS

In this paper we have described a new approach for PDK re-centering based on TCAD and experimental data at cryogenic temperatures suitable for circuit design applications in data centers and quantum computers. A similar procedure can be used to derive target data for cryogenic compact model extraction for SS and FF corners. Further work is in progress to extend this methodology for deriving statistical SPICE models, which are essential for verifying circuit performance at cryogenic temperatures.

## ACKNOWLEDGEMENT

We are grateful to GlobalFoundries for providing the 22FDX PDK and allowing us to customize it for cryogenic

temperature operation. The device measurements were performed by Incize SRL, Belgium. This work was supported partially by Innovate UK funded project ‘‘Development of Cryo-CMOS to enable the next generation of scalable quantum computers’’ under the grant number of 10006017 and was also partially supported by Semiwise Ltd, UK.

## REFERENCES

- [1] E. Charbon, F. Sebastiano, A. Vladimirescu, H. Homulle, S. Visser *et al.*, ‘‘Cryo-CMOS for quantum computing,’’ in *2016 IEEE International Electron Devices Meeting (IEDM)*, Dec 2016, pp. 13.5.1–13.5.4. DOI: 10.1109/IEDM.2016.7838410
- [2] X. Xue, B. Patra, J. van Dijk *et al.*, ‘‘CMOS-based cryogenic control of silicon quantum circuits,’’ *Nature*, vol. 593, pp. 205–210, 2021. DOI: 10.1038/s41586-021-03469-4
- [3] L. Wang, B. Cheng, P. Asenov, A. Pender, D. Reid *et al.*, ‘‘TCAD proven compact modelling re-centering technology for early 0.x PDKs,’’ in *2016 International Conference on Simulation of Semiconductor Processes and Devices (SISPAD)*, Sep 2016, pp. 157–160. DOI: 10.1109/SISPAD.2016.7605171
- [4] S. C. Jung, H.-C. Joo, S. Yi, Y. Kim, and Y.-H. Hwang, ‘‘Compact characteristic modeling of cryo-cmos transistors based on commercial process design kit,’’ in *2024 International Conference on Electronics, Information, and Communication (ICEIC)*, 2024, pp. 1–3. DOI: 10.1109/ICEIC61013.2024.10457101
- [5] S. K. Singh, P. Malviya, and A. Dixit, ‘‘Developing process design kit (q-pdk) for co-integrated quantum computers,’’ in *2024 IEEE Latin American Electron Devices Conference (LAEDC)*, 2024, pp. 1–4. DOI: 10.1109/LAEDC61552.2024.10555760
- [6] A. Akturk, A. Tripathi, and M. Saligane, ‘‘Cryogenic modeling for open-source process design kit technology,’’ in *2023 IEEE BiCMOS and Compound Semiconductor Integrated Circuits and Technology Symposium (BCICTS)*, 2023, pp. 58–65. DOI: 10.1109/BCICTS54660.2023.10310944
- [7] Synopsys Inc, *Sentaurus Process User Guide*, Mountain View, CA, USA, 2022.
- [8] Synopsys Inc, *Sentaurus Device Manual*, Mountain View, CA, USA, 2022.
- [9] D. Klaassen, ‘‘A unified mobility model for device simulation—i. model equations and concentration dependence,’’ *Solid-State Electronics*, vol. 35, no. 7, pp. 953–959, 1992. DOI: 10.1016/0038-1101(92)90325-7
- [10] C. Lombardi, S. Manzini, A. Saporito, and M. Vanzi, ‘‘A physically based mobility model for numerical simulation of nonplanar devices,’’ *IEEE Transactions on Computer-Aided Design of Integrated Circuits and Systems*, vol. 7, no. 11, pp. 1164–1171, 1988. DOI: 10.1109/43.9186
- [11] W. Hansch, T. Vogelsang, R. Kircher, and M. Orlowski, ‘‘Carrier transport near the Si/SiO<sub>2</sub> interface of a MOSFET,’’ *Solid-State Electronics*, vol. 32, pp. 839–849, October 1989. DOI: 10.1063/1.337408
- [12] R. Carter, J. Mazurier, L. Pirro, J.-U. Sachse, P. Baars *et al.*, ‘‘22nm fdsoi technology for emerging mobile, internet-of-things, and rf applications,’’ in *2016 IEEE International Electron Devices Meeting (IEDM)*, 2016, pp. 2.2.1–2.2.4. DOI: 10.1109/IEDM.2016.7838029
- [13] E. O. Kane, ‘‘Thomas-Fermi approach to impure semiconductor band structure,’’ *Phys. Rev.*, vol. 131, pp. 79–88, Jul 1963. DOI: 10.1103/PhysRev.131.79
- [14] ‘‘BSIM compact models.’’ [Online] <https://bsim.berkeley.edu/models/>
- [15] Synopsys Inc, *HSPICE User Guide*, Mountain View, CA, USA, 2022.